


# Transitory presence of myeloid-derived suppressor cells in neonates is critical for control of inflammation

Yu-Mei He<sup>1,2,9</sup>, Xing Li<sup>1-3,9</sup>, Michela Perego<sup>4,9</sup> , Yulia Nefedova<sup>4</sup>, Andrew V Kossenkov<sup>4</sup>, Erik A Jensen<sup>5</sup>, Valerian Kagan<sup>6</sup>, Yu-Feng Liu<sup>1</sup>, Shu-Yu Fu<sup>1</sup>, Qing-Jian Ye<sup>3</sup>, Yan-Hong Zhou<sup>7</sup>, Lai Wei<sup>8</sup>, Dmitry I Gabrilovich<sup>1,2,4,10</sup> & Jie Zhou<sup>1,2,7,10</sup>

Myeloid-derived suppressor cells (MDSCs) are pathologically activated and relatively immature myeloid cells that have been implicated in the immunological regulation of many pathologic conditions<sup>1,2</sup>. Phenotypically and morphologically, MDSCs are similar to neutrophils (PMN-MDSCs) and monocytes (M-MDSCs). However, they have potent suppressive activity and distinct gene expression profiles and biochemical characteristics<sup>3</sup>. No or very few MDSCs are observed in steady-state physiological conditions. Therefore, until recently, accumulation of MDSCs was considered a consequence of pathological processes or pregnancy. Here, we report that MDSCs with a potent ability to suppress T cells are present during the first weeks of life in mice and humans. MDSC suppressive activity was triggered by lactoferrin and mediated by nitric oxide, PGE<sub>2</sub>, and S100A9 and S100A8 proteins. MDSCs from newborns had a transcriptome similar to that of tumor MDSCs, but with strong upregulation of an antimicrobial gene network, and had potent antibacterial activity. MDSCs played a critical role in control of experimental necrotizing enterocolitis (NEC) in newborn mice. MDSCs in infants with very low weight, who are prone to NEC, had lower MDSC levels and suppressive activity than did infants with normal weight. Thus, the transitory presence of MDSCs may be critical for regulation of inflammation in newborns.

Although MDSCs are largely absent in healthy adults, recent evidence has indicated that MDSCs may play a role in the maintenance of maternal–fetal tolerance<sup>4</sup>. The roles of MDSCs in pregnancy appear to be consistent with a myeloid-cell response to partial genetic incomparability between mother and child. In this study, we tested the possible roles of MDSCs in steady-state conditions during the first weeks of life.

Populations of myeloid cells were evaluated in the spleens and bone marrow (BM) of adult mice (AM; 6–8 weeks of age), newborn mice (NBM), and adult mice within 7 d after giving birth (postpartum

mice, PM). In comparison to AM and PM, 7- to 10-d-old NBM had substantially more splenic CD11b<sup>+</sup>Ly6C<sup>hi</sup>Ly6G<sup>−</sup> monocytes and CD11b<sup>+</sup>Ly6C<sup>lo</sup>Ly6G<sup>+</sup> neutrophils (Supplementary Fig. 1a). Cells from NBM and AM had similar morphology (Supplementary Fig. 1b). The proportion of these populations was highest on day 1 after birth and gradually decreased to levels comparable to those in AM by the end of week 2 (Fig. 1a). The population of spleen macrophages was not different, whereas dendritic cells were lower in NBM than AM (Supplementary Fig. 1c). In contrast to those in AM, monocytes from 7- to 10-d-old NBM potently inhibited proliferation of CD4<sup>+</sup> and CD8<sup>+</sup>T cells (Fig. 1b), and neutrophils demonstrated potent suppression of antigen-specific proliferation of CD8<sup>+</sup> T cells (Fig. 1c). Thus, these cells fit the criteria of M-MDSCs and PMN-MDSCs, respectively<sup>3</sup>. In NBM, MDSC suppressive activity was not observed during the first 3 d and disappeared after day 14 (Fig. 1d,e). Spleen macrophages did not have suppressive activity (Supplementary Fig. 1d). In lactating PM, the number of monocytes and neutrophils did not differ from that in AM, and no suppressive activity was detected (Supplementary Fig. 1e–h). Thus, MDSCs were found exclusively in NBM.

To assess the ability of NBM MDSCs to control autoimmune inflammation, AM were sensitized and challenged with intranasal administration of ovalbumin (OVA) (Supplementary Fig. 2a). Administration of NBM MDSCs, but not AM neutrophils, decreased lung inflammation (Supplementary Fig. 2b,c), the presence of leukocytes, and the amounts of IL-13 and IL-4 in bronchoalveolar lavage (Supplementary Fig. 2d–g), and IgE in sera (Supplementary Fig. 2h).

CD11b<sup>+</sup>Ly6C<sup>lo</sup>Ly6G<sup>+</sup> and CD11b<sup>+</sup>Ly6C<sup>hi</sup>Ly6G<sup>−</sup> cells from the spleens of AM and 7-d-old NBM were sorted, and whole transcriptome analysis was performed through RNA-seq (Supplementary Fig. 3a). Ingenuity Pathway Analysis (IPA) revealed upregulation of 55 key transcriptional regulators in NBM including lactoferrin (*Ltf*), *S100a8*, and *S100a9*. Prostaglandin E synthase (*Ptges*) was upregulated in PMN-MDSCs. *Ptges* controls synthesis of the prostaglandin PGE<sub>2</sub>,

<sup>1</sup>Institute of Human Virology, Zhongshan School of Medicine, Sun Yat-sen University, Guangzhou, China. <sup>2</sup>Key Laboratory of Tropical Disease Control, Chinese Ministry of Education, Guangzhou, China. <sup>3</sup>Third Affiliated Hospital, Sun Yat-sen University, Guangzhou, China. <sup>4</sup>Wistar Institute, Philadelphia, Pennsylvania, USA. <sup>5</sup>Children's Hospital of Philadelphia, Philadelphia, Pennsylvania, USA. <sup>6</sup>Department of Environmental and Occupational Health, University of Pittsburgh, Pittsburgh, Pennsylvania, USA. <sup>7</sup>Guangzhou Women and Children's Medical Center, Guangzhou, China. <sup>8</sup>Zhongshan Ophthalmic Center, Sun Yat-sen University, Guangzhou, China. <sup>9</sup>These authors contributed equally to this work. <sup>10</sup>These authors jointly directed this work. Correspondence should be addressed to D.I.G. (dgabrilovich@wistar.org) or J.Z. (zhouj72@mail.sysu.edu.cn).

Received 11 January 2017; accepted 12 December 2017; published online 15 January 2018; doi:10.1038/nm.4467

which has been implicated in MDSC function<sup>5,6</sup> (Supplementary Fig. 3b). In a previous study, we evaluated the transcriptional profiles of MDSCs in tumor-bearing mice<sup>7</sup>. Gene expression profiles in NBM MDSCs did not correlate with those of neutrophils and monocytes from tumor-free mice but showed correlations with those of cells from tumor-bearing mice (Supplementary Fig. 3c). Notably, 'antimicrobial response' was the most prominent network found by IPA in NBM MDSCs (Supplementary Fig. 3d). NBM PMN-MDSCs exhibited more killing of *Escherichia coli* and *Candida albicans* than did AM neutrophils, and NBM M-MDSCs were more potent in killing *E. coli* than were AM monocytes (Supplementary Fig. 4a,b).

Our experiments indicated that NBM M-MDSCs and PMN-MDSCs used different mechanisms of immunosuppression. Upregulation of *Nos2* and nitric oxide (NO) was responsible for suppression by M-MDSCs (Supplementary Fig. 5a,b), whereas upregulation of *S100A9* and *S100A8* (*S100A9/A8*) was responsible for suppression by NBM PMN-MDSCs (Fig. 1f–h). In the absence of these proteins in *S100A9*-knockout (KO) mice<sup>8</sup>, NBM neutrophils lacked suppressive activity, whereas NBM M-MDSCs retained this activity (Fig. 1h). Although *S100A9/A8* are known to associate with MDSCs, the specific mechanisms by which these proteins affect the suppressive activity of MDSCs were unclear. On the basis of gene profiling data, we focused on *Ptges*, which is required for terminal PGE<sub>2</sub> synthesis<sup>9</sup>. Upregulation of *Ptges* in NBM PMN-MDSCs was abrogated in *S100A9*-KO mice (Fig. 1i), thus suggesting that *S100A9* regulates *Ptges*. NBM PMN-MDSCs from 7-d-old mice, but not from 3-d-old mice, produced a substantially higher amount of PGE<sub>2</sub> than did neutrophils from AM. Notably, NBM PMN-MDSCs from *S100A9*-KO mice had a low amount of PGE<sub>2</sub> similar to that in AM neutrophils (Fig. 1j), thus indicating that *S100A9/A8* are involved in PGE<sub>2</sub> synthesis via regulation of *Ptges*. In NBM PMN-MDSCs and AM neutrophils, the expression of *Cox-2* (official symbol *Ptgs2*) was similar (Supplementary Fig. 5c). NBM PMN-MDSCs from *Cox-2*-KO mice lacking PGE<sub>2</sub> production (Supplementary Fig. 5d), compared with wild-type (WT) mice, had a substantially lower ability to suppress antigen-specific T-cell proliferation (Fig. 1k). Thus, PMN-MDSC activity in NBM was regulated by the *S100A9/A8*-mediated upregulation of *Ptges* and PGE<sub>2</sub> production.

The detection of immunosuppressive MDSCs in NBM between days 4 and 14 might suggest a role of microbial colonization of the gut, which takes place during this period<sup>10</sup>. However, treatment of pregnant mice with combinations of antibiotics that depleted gut microbiota (Supplementary Fig. 6a,b) did not affect the presence or suppressive activity of MDSCs (Supplementary Fig. 6c–e).

We hypothesized that accumulation of MDSCs in NBM might be linked with milk feeding. Hence, we tested the effect of lactoferrin (LF), a milk component with potent immunoregulatory activity<sup>11</sup>, on myeloid cells *in vivo* by treating 3-week-old mice with daily intraperitoneal (i.p.) administration of LF. Eight-day treatment resulted in an increase in suppressive MDSCs (Fig. 2a–c). Treatment of 6-week-old mice with LF did not induce an increase in suppressive MDSCs, thus suggesting that myeloid progenitors differ in susceptibility to LF in mice at different ages. LF mediated suppression via *Nos2* and NO in M-MDSCs (Fig. 2d,e) and via upregulation of *S100a8* and *S100a9* (Fig. 2f,g) and PGE<sub>2</sub> (Fig. 2h) in PMN-MDSCs. Treatment of *S100A9*-KO mice with LF did not induce immunosuppressive PMN-MDSCs (Fig. 2i). In the absence of LF in LF-KO mice, the granulocytes had no suppressive activity (Fig. 2j) and exhibited lower *S100A9* protein content (Fig. 2k), *Ptges* expression (Fig. 2l), and PGE<sub>2</sub> content (Fig. 2m) than did PMN-MDSCs from WT NBM. Together, these

data indicated that LF may be a major factor causing acquisition of immunosuppressive activity by MDSCs in NBM.

Because myeloid cells produce LF (Supplementary Fig. 7a), we sought to determine the source of LF that drives MDSC accumulation by performing cross-fostering experiments. Cross-fostering of WT mice with LF-KO surrogates did not result in generation of immunosuppressive PMN-MDSCs. In contrast, cross-fostering of LF-KO NBM with WT mice generated immunosuppressive PMN-MDSCs (Supplementary Fig. 7b). No differences in the total number of CD11b<sup>+</sup>Ly6C<sup>lo</sup>Ly6G<sup>+</sup> cells were found (Supplementary Fig. 7c). These results indicated that LF in milk has a role in MDSC generation.

We hypothesized that MDSCs might be important for the control of inflammation associated with early microbial colonization in neonates. One of the manifestations of pathological inflammation in neonates is necrotizing enterocolitis (NEC), which is characterized by acute intestinal injury with an associated systemic inflammatory response that may result from the establishment of gut microbiota<sup>12</sup>. NEC develops in 7–11% of infants with birth weights <1,500 g, termed very low weight (VLW) infants. The estimated mortality rate due to NEC is nearly 30% and approaches 100% among those with the most severe form, NEC totalis. Abnormalities in immune responses have been suggested to play a critical role in the development of NEC<sup>13</sup>. We investigated differences in MDSCs from the peripheral blood of normal weight (NW) (>2,500 g) or VLW (<1,500 g) newborn infants. In peripheral blood mononuclear cells (PBMCs), healthy adults had very few cells with the phenotype and morphology of PMN-MDSCs (CD11b<sup>+</sup>CD14<sup>+</sup>CD15<sup>+</sup>) or M-MDSCs (CD11b<sup>+</sup>CD14<sup>+</sup>HLA-DR<sup>+/lo</sup>CD15<sup>+</sup>) (Fig. 3a and Supplementary Fig. 8). The frequencies of MDSCs in NW infants were substantially higher than those in adults and VLW babies (Fig. 3a). MDSCs from NW infants had more potent suppressive activity than did cells from VLW babies (Fig. 3b). To verify these findings, we evaluated the presence of LOX-1<sup>+</sup> neutrophils in infants. In cancer patients, LOX-1<sup>+</sup>CD15<sup>+</sup> neutrophils have been found to represent a population of PMN-MDSCs<sup>14</sup>. Only LOX-1<sup>+</sup> but not LOX-1<sup>−</sup> neutrophils from NW infants suppressed T cell function (Fig. 3c). In infants, the proportion of LOX-1<sup>+</sup> PMN-MDSCs was much higher than that in adults (Fig. 3d), and the frequency of these cells was lower in VLW than in NW infants (Fig. 3e). Treatment with the NOS2 inhibitor LNMA, but not reactive oxygen species (ROS) inhibitors, cancelled the suppressive activity of M-MDSCs (Fig. 3f). M-MDSCs from NW infants but not from VLW infants had higher NOS2 expression (Fig. 3g) and produced more nitrites (Fig. 3h) than did adult monocytes. PMN-MDSCs from NW infants had markedly higher production of PGE<sub>2</sub> (Fig. 3i) and expression of *S100A9* mRNA (Fig. 3j), *S100A9* protein (Fig. 3k), and *LTF* mRNA (Fig. 3l) than did cells from adults and VLW infants. MDSCs from NW and VLW neonates had higher antibacterial activity than did neutrophils and monocytes from adults (Supplementary Fig. 9). NW infants fed with breast milk had higher levels of LOX-1<sup>+</sup> PMN-MDSCs than did infants who received formula lacking LF (Fig. 3m).

We next asked whether MDSCs might be important in NEC. We used a gavage/hypoxia experimental model of NEC<sup>15</sup>, which manifests as inflammatory gut injury of varying intensity (Fig. 4a). Although this model, like other models of NEC, cannot fully recapitulate human disease, it generates conditions (intestinal necrosis and inflammation) similar to those observed in humans. Induction of NEC in 1-d-old mice with NBM (with no MDSCs present) caused much more severe inflammation than that in 4-day-old mice with NBM (with MDSCs present), which manifested as higher intestine

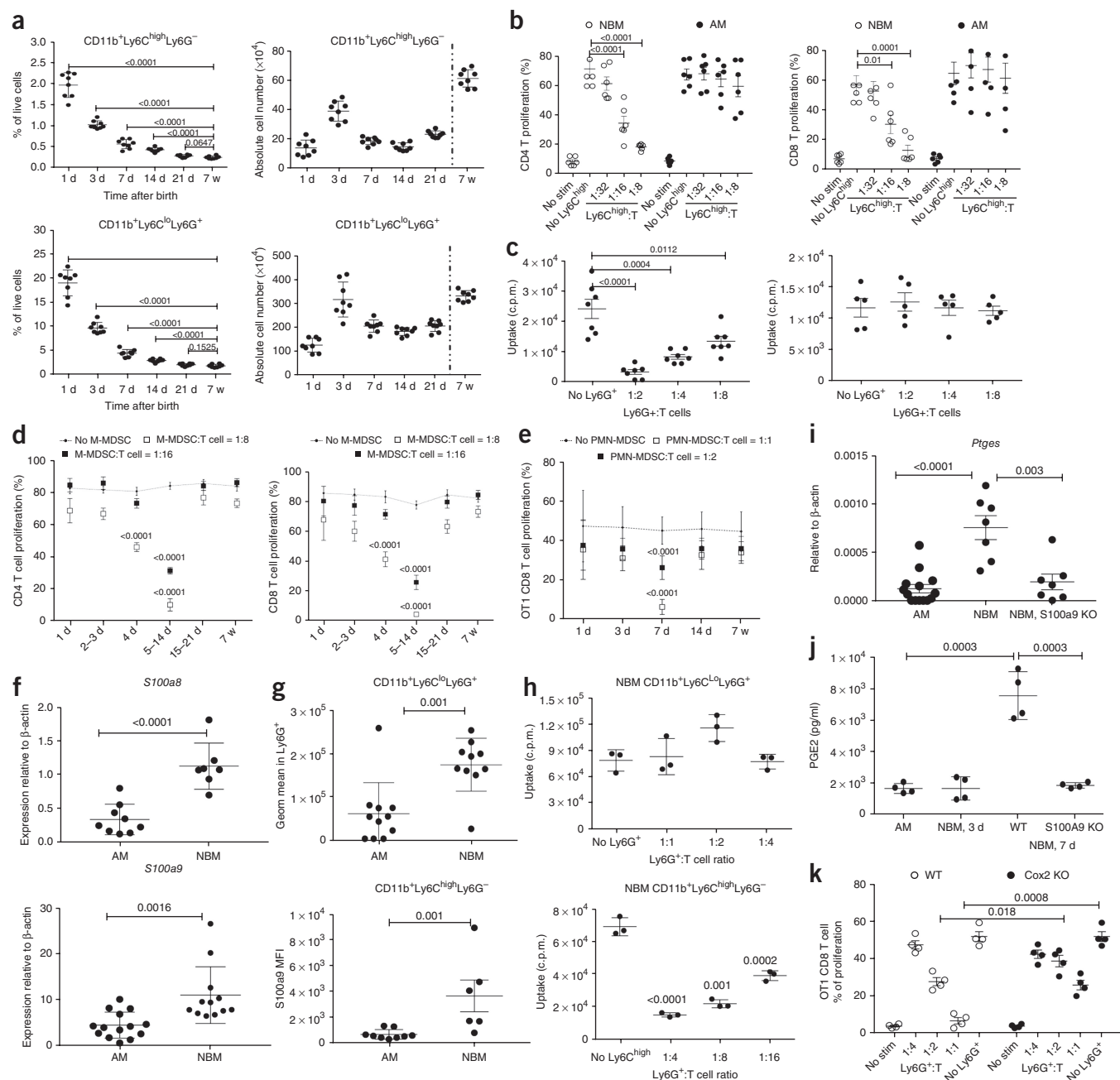


**Figure 1** Expansion of MDSCs in NBM. **(a)** Proportion and absolute number of the populations of splenocytes at different times after birth ( $n = 8$  mice). 'w' denotes weeks. In AM, the total number of splenic cells could not be directly compared with that in NBM, owing to the much larger spleen size. These results are provided for reference only. **(b)** CD3/CD28-inducible proliferation of CD4<sup>+</sup> (from  $n = 6$  mice) and CD8<sup>+</sup> (from  $n = 4$  mice) T cells in the presence of M-MDSCs isolated from NBM and AM. No stim, unactivated T cells (negative control); no MDSC, T cell proliferation in the absence of MDSCs. Proliferation was measured through carboxyfluorescein succinimidyl ester (CFSE) dilution. **(c)** Antigen-specific proliferation of CD8<sup>+</sup> T cells in the presence of PMN-MDSCs isolated from NBM and AM. Proliferation was measured in triplicate through <sup>3</sup>H[thymidine] uptake. OT-1 T cells were used as responders in antigen-specific suppression assays. Experiments were performed in triplicate, and individual experiments are shown. Left, NBM ( $n = 7$ ); right, AM ( $n = 5$ ). **(d)** Antigen nonspecific suppression assays of M-MDSCs isolated from newborn spleen at different time points after birth ( $n = 4$  mice). **(e)** Antigen-specific suppression assays of PMN-MDSCs isolated from newborn spleen at different time points after birth ( $n = 4$  mice). **(f)** *S100a8* ( $n = 8$  AM,  $n = 7$  NBM) and *S100a9* ( $n = 14$  AM,  $n = 12$  NBM) gene expression in PMN-MDSCs from 7-d-old NBM and AM. **(g)** Intracellular S100A9 protein expression measured by flow cytometry in PMN-MDSCs ( $n = 11$  AM,  $n = 10$  NBM) or M-MDSCs ( $n = 9$  AM,  $n = 6$  NBM) from 7-d-old NBM or AM. There are differences in the scale of mean fluorescence intensity (MFI) between PMN-MDSCs and M-MDSCs. Geom, geometric. **(h)** Antigen-specific suppression assays of PMN-MDSCs and M-MDSCs isolated from the spleens of 7-d-old S100A9-KO mice. Cell proliferation was measured in triplicate on the basis of <sup>3</sup>H[thymidine] uptake. A typical example from three experiments is shown. **(i)** *Ptgcs* gene expression in PMN-MDSCs (qRT-PCR). NBM ( $n = 7$ ), newborn S100A9-KO ( $n = 7$ ), AM control ( $n = 14$ ). **(j)** Amount of PGE2 measured by ELISA in cell supernatants from 24-h culture of PMN-MDSCs from adult and newborn (3 d or 7 d old) WT mice or S100a9-KO 7-d-old NBM ( $n = 4$ ). **(k)** Antigen-specific suppression assay of PMN-MDSCs isolated from spleens of 7-d-old newborn WT and Cox-2-KO mice ( $n = 4$ ). In all plots, mean  $\pm$  s.d. are shown. In most panels,  $P$  values from two-tailed Student's  $t$  tests are shown.

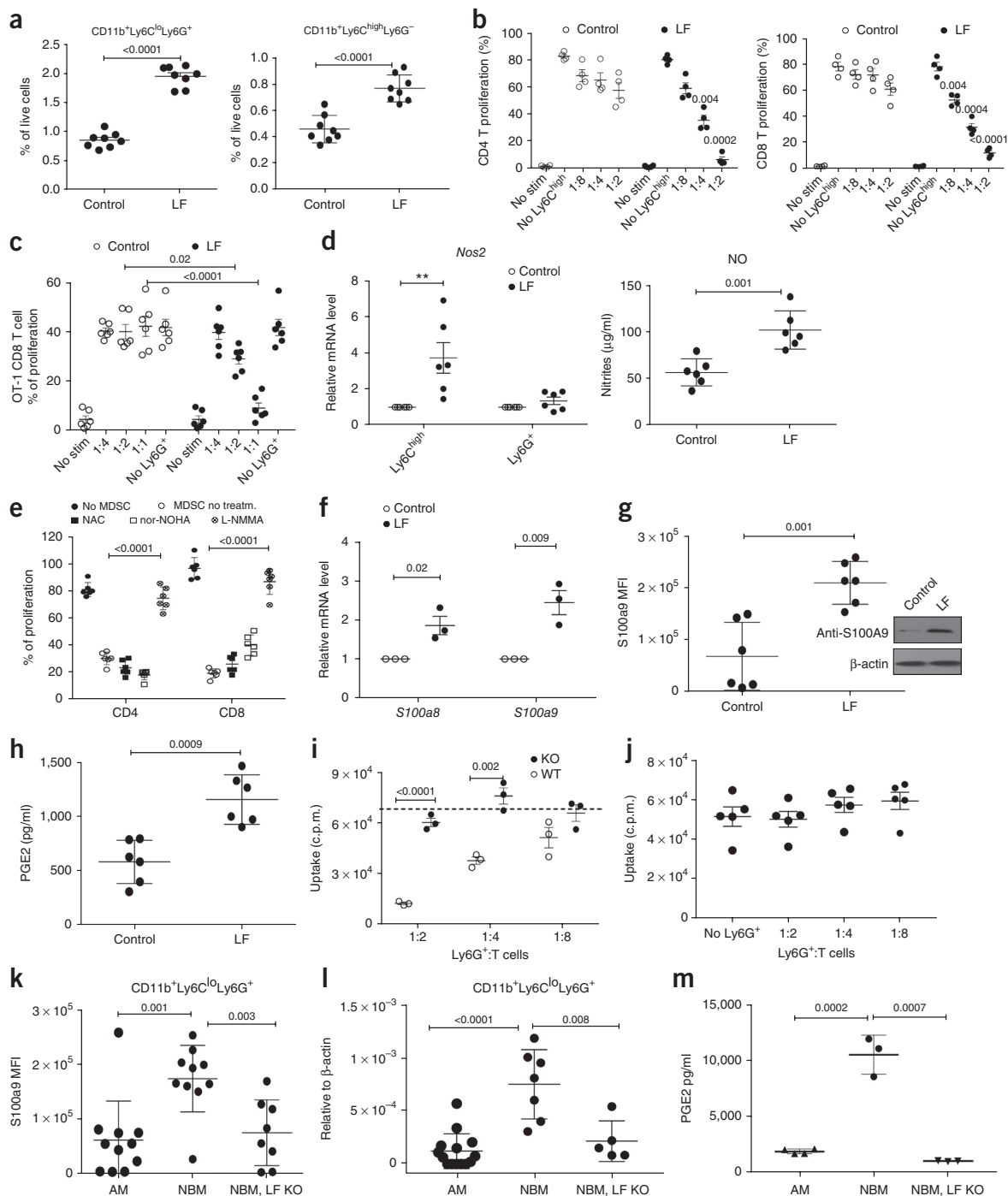


**Figure 2** Lactoferrin is responsible for accumulation of MDSCs in NBM. (a) Proportion of monocytes and neutrophils in LF-treated 3-week-old mice ( $n = 8$ ). Control, mice treated with PBS. (b) Suppression of CD3/CD28-stimulated T cells by M-MDSCs isolated from AM treated with LF or PBS (control) ( $n = 4$ ). (c) Antigen-specific suppression assay of PMN-MDSCs isolated from AM treated with LF ( $n = 6$ ). (d) Expression of *Nos2* in MDSCs from LF-treated mice ( $n = 6$ ) (left). Amount of NO in M-MDSCs from LF-treated mice ( $n = 6$ ) (right). (e) Suppression of CD3/CD28-stimulated T cells by M-MDSCs from LF-treated mice ( $n = 6$ ) in the presence of inhibitors of ROS (NAC), arginase I (nor-NOHA), or *Nos2* (L-NMMA). (f) Expression of *S100a9* and *S100a8* genes in PMN-MDSCs from LF-treated mice ( $n = 3$ ). (g) Mean fluorescence intensity (MFI) of intracellular expression of S100A9 protein detected by flow cytometry in PMN-MDSCs from AM treated with LF ( $n = 6$ ). Inset, amount of S100A9 protein detected by western blotting. Representative results from three independent experiments are shown. (h) PGE2 amounts in cell lysates from 24-h cultures of PMN-MDSCs isolated from AM treated with LF ( $n = 6$ ). (i) Antigen-specific T cell-suppressive activity of PMN-MDSCs isolated from LF-treated WT and S100A9-KO mice. Proliferation was measured as  $^3\text{H}$ [thymidine] uptake in triplicate. Representative results from three experiments are shown. Dotted line, level of T cell proliferation in the absence of MDSCs. (j) Antigen-specific suppression assays of PMN-MDSCs isolated from LF-KO mice. Experiments were performed in triplicate. Results of 5 experiments are shown. (k) MFI of intracellular S100A9 protein expression in PMN-MDSCs in AM ( $n = 11$ ), newborn WT ( $n = 10$ ), and LF-KO ( $n = 8$ ) mice. (l) Expression of *Ptges* in PMN-MDSCs from AM ( $n = 13$ ), newborn WT ( $n = 7$ ), and LF-KO ( $n = 5$ ) mice. (m) Amount of PGE2 measured by ELISA in cell lysates from 24-h cultures of PMN-MDSCs from AM ( $n = 4$ ) and NBM WT ( $n = 3$ ) or LF-KO NBM ( $n = 3$ ). In all plots, mean  $\pm$  s.e.m. are shown.  $P$  values from two-tailed Student's  $t$  tests are shown.

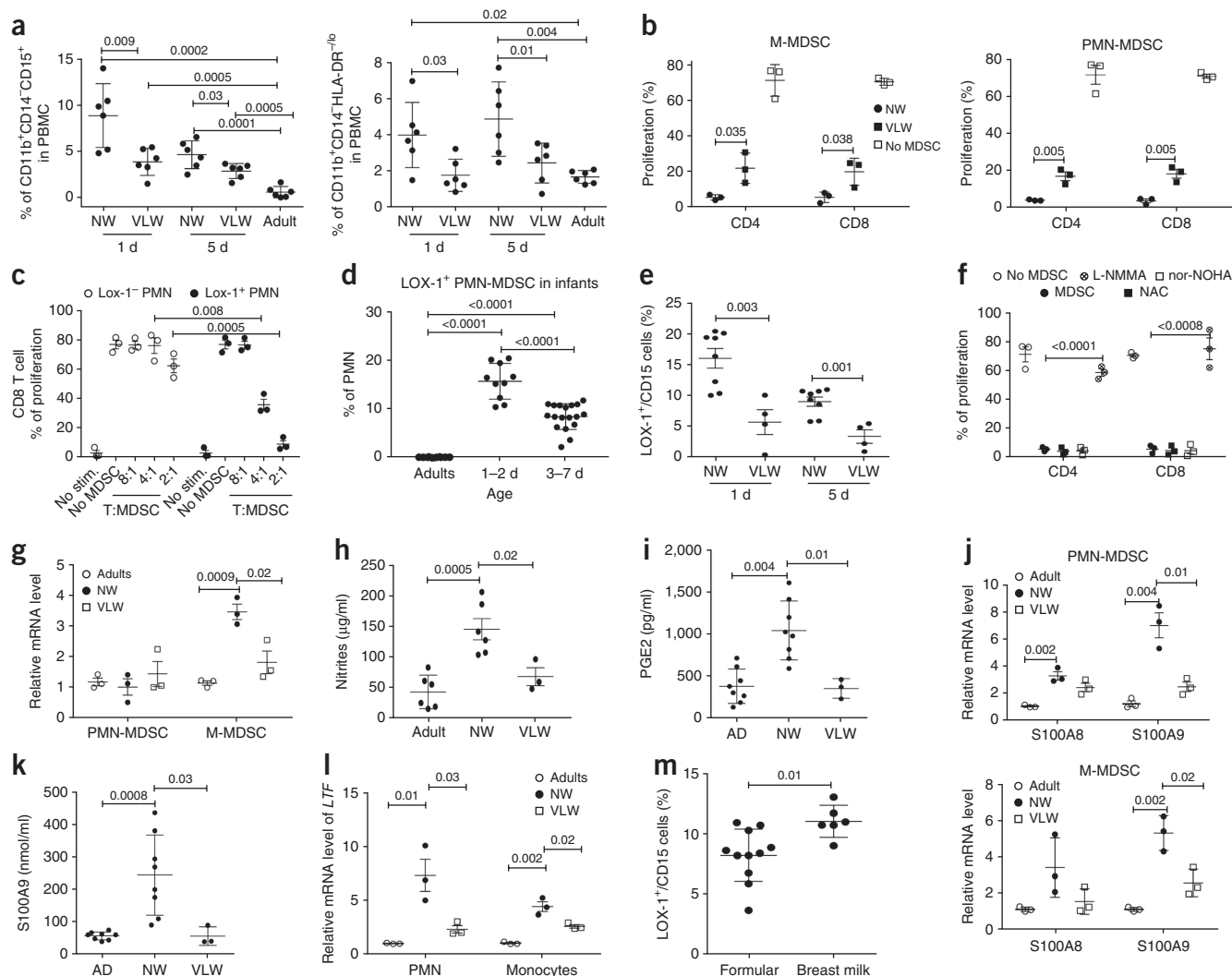


**Figure 3** MDSCs in human infants. (a) Proportion of MDSCs in peripheral blood of infants. PMN-MDSCs (left) and M-MDSC (right) were evaluated in PBMCs from peripheral blood of NW and VLW infants ( $n = 6$ ) at the indicated times after birth. Individual data and s.d. are shown. (b) Functional activity of MDSCs from infants. M-MDSCs and PMN-MDSCs were sorted from PBMCs of NW and VLW infants and added to T cells isolated from blood and stimulated with antibodies to CD3/CD28. Proliferation was measured in triplicate through CFSE labeling. (c–e) LOX-1<sup>+</sup> PMN-MDSCs in newborns. (c) LOX-1<sup>+</sup> and LOX-1<sup>-</sup> CD15<sup>+</sup> cells were isolated from peripheral blood of newborn infants and tested in suppressive activity against CD3/CD28-stimulated T cells. Proliferation was measured in triplicate through CFSE staining. (d) Proportion of LOX-1<sup>+</sup> cells among CD15<sup>+</sup> neutrophils in infants of different ages (1–2 d ( $n = 10$ ), 3–7 d ( $n = 18$ )) and in adults ( $n = 7$ ). Individual results and s.d. are shown. (e) Proportion of LOX-1<sup>+</sup> cells in NW ( $n = 8$ ) and VLW ( $n = 4$ ) infants of different ages. Individual results are shown. (f–l) Mechanisms regulating MDSC activity in infants. Samples of blood were collected from newborn infants 1–5 d after birth. M-MDSCs and PMN-MDSCs were sorted from PBMCs. (f) Suppressive activity of M-MDSCs from NW infants in the presence of inhibitors of ROS (NAC), arginase I (nor-NOHA), or NOS2 (L-NMMA). Effectors were CD4<sup>+</sup> or CD8<sup>+</sup> T cells stimulated with antibodies to CD3/CD28. Proliferation was measured in triplicate through CFSE staining. (g) Expression of *NOS2* in M-MDSCs ( $n = 3$  individuals). (h) Nitrites produced by M-MDSCs. NW ( $n = 6$  individuals), VLW ( $n = 3$  individuals), control cells from adults ( $n = 6$  individuals). Individual results are shown as means and s.d. (i) The amount of PGE2 produced by PMN-MDSCs and measured by ELISA in cell lysates. NW and adults ( $n = 8$  individuals), VLW ( $n = 3$  individuals). Individual results are shown as mean and s.d. (j) Expression of *S100A8* and *S100A9* in PMN-MDSCs and M-MDSCs measured by qPCR ( $n = 3$  individuals). (k) The amount of S100A9 protein in cell lysates of PMN-MDSCs. NW ( $n = 8$  infants), VLW ( $n = 3$  infants), adults ( $n = 8$  individuals). (l) Expression of *LTF* in PMN-MDSCs and M-MDSCs ( $n = 3$  individuals). (m) LOX-1<sup>+</sup> PMN-MDSCs in blood of 5-d-old infants receiving formula ( $n = 11$ ) or mother's milk ( $n = 6$ ). In all panels, mean  $\pm$  s.d. are shown.  $P$  values from two-tailed Student's  $t$  tests are shown.

permeability (Fig. 4b), higher inflammation scores (Fig. 4c), and shorter survival times (Fig. 4d). The differences in bacterial load were small but significant ( $P = 0.018$ ) (Fig. 4e).

To selectively deplete MDSCs in these mice, we used an agonistic antibody to TRAIL-R (DR5ab)<sup>16–18</sup>. PMN-MDSCs in NBM had higher expression of DR5 than did neutrophils from AM (Supplementary Fig. 10a). The population of MDSCs in the lamina propria (LP) was substantially lower in DR5ab-treated cells than in control cells

(Supplementary Fig. 10b and Fig. 4f). DR5ab significantly ( $P = 0.03$ ) shortened survival (Fig. 4g) and increased inflammation scores (Fig. 4h) and intestine permeability (Fig. 4i). Moreover, this treatment resulted in a small but significant ( $P = 0.045$ ) increase in bacterial load in the intestine (Fig. 4j) and blood (Fig. 4k). S100A9-KO mice were much more sensitive than WT mice to NEC induction (Supplementary Fig. 10c), thus indicating the important role of S100A9 in PMN-MDSC protection in NEC.

We next tested the effects of transfer of MDSCs from NBM on NEC development. After transfer to mice with NEC, MDSCs were readily detectable in the intestine (**Supplementary Fig. 10d,e**). MDSCs from

NBM elicited a decrease in inflammation scores (**Fig. 4l**) and intestinal permeability (**Fig. 4m**). In contrast, Gr-1<sup>+</sup> cells from AM had no effect on gut inflammation (**Fig. 4l,m**). Injection of AM cells did not

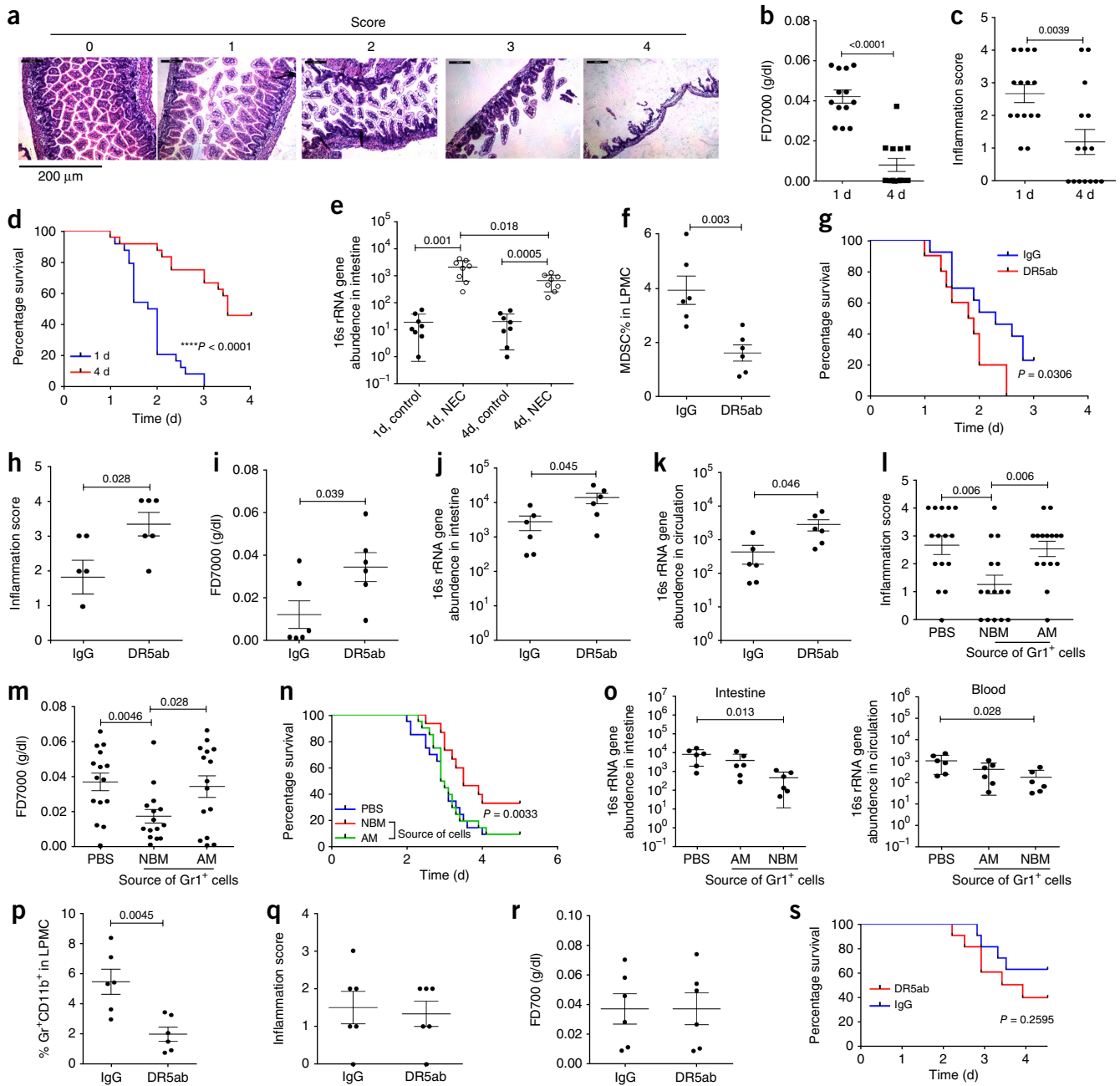


**Figure 4** Role of MDSCs in a necrotizing enterocolitis (NEC) experimental model. **(a)** Representative images (from 5 performed) of mouse intestine after NEC induction. Numbers in the pictures indicate NEC severity from 0 (normal epithelium) to 4 (most severe NEC). **(b–d)** Detection of fluorescein isothiocyanate-labeled dextran (FD7000) (directly proportional to intestine permeability) ( $n = 13$  mice) **(b)**, small intestine inflammation score ( $n = 15$ ) **(c)**, and survival ( $n = 24$ ) **(d)** in 1- and 4-day-old mice after NEC induction. **(e)** Bacterial load in the small intestine in mice ( $n = 8$ ) evaluated on the basis of 16s rRNA gene abundance. **(f)** Flow cytometry analysis of MDSC presence in the LP after MDSC depletion with DR5ab ( $n = 6$  mice). **(g)** Survival analysis of WT NEC mice subjected to MDSC depletion by DR5ab treatment ( $n = 13$ ) or treated with IgG ( $n = 10$ ). **(h)** Small intestine inflammation score in 6-day-old mice after MDSC depletion (IgG,  $n = 5$ ; DR5,  $n = 6$ ). **(i)** FD7000 after MDSC depletion ( $n = 6$  mice). **(j,k)** Bacterial load evaluated in the intestine ( $n = 6$  mice) **(j)** and blood ( $n = 6$  mice) **(k)**. Bacterial load was normalized to the levels in NBM without NEC. Values for individual mice are shown. **(l–n)** Inflammation scores in the small intestine in NBM after treatment with exogenous Gr1<sup>+</sup> cells from NBM, AM, or vehicle control (PBS) ( $n = 15$  mice) **(l)**, intestine permeability ( $n = 15$  mice) **(m)**, and survival of mice **(n)** after NEC induction and treatment with Gr1<sup>+</sup> cells from NBM ( $n = 20$  mice), AM ( $n = 15$  mice) or vehicle control (PBS) ( $n = 15$  mice). **(o)** Bacterial load evaluated in the intestine and blood ( $n = 6$  mice). **(p)** Flow cytometry analysis of MDSC presence in the LP in Rag1-KO mice with induced NEC treated with DR5ab or control IgG ( $n = 6$ ). **(q)** Small-intestine inflammation scores for Rag1-KO mice with induced NEC treated with DR5ab ( $n = 6$ ). **(r)** FD7000 in mice treated with DR5ab ( $n = 6$ ). **(s)** Survival analysis of mice treated with DR5ab or IgG after NEC induction ( $n = 11$ ). Individual values are shown with s.d. In all panels, mean and s.d. are shown.  $P$  values from two-tailed Student's  $t$  test are shown.

affect the survival of mice with NEC. In contrast, MDSCs from NBM substantially prolonged survival (Fig. 4n). Transfer of MDSCs from NBM decreased the bacterial load in both the intestine and blood. However, no differences in the effects of MDSC and Gr-1<sup>+</sup> cells from AM on bacterial load were detected (Fig. 4o).

Thus, it appears that the antibacterial effect of MDSCs is not a major factor in their effect on NEC. To confirm this possibility, we used Rag1-KO mice lacking T and B cells. In agreement with findings from previous reports<sup>19</sup>, NEC in Rag1-KO mice had lower inflammation and longer survival times than did WT mice (Supplementary Fig. 10f–i). However, no differences in bacterial load were evident (Supplementary Fig. 10j,k). Depletion of MDSCs in Rag1-KO mice (Supplementary Fig. 10l and Fig. 4p) did not affect the inflammation scores (Fig. 4q), intestine permeability (Fig. 4r), or survival of the mice (Fig. 4s). Depletion of MDSCs did not affect the bacterial load in the intestine or blood in Rag1-KO mice (Supplementary Fig. 10m).

We then induced NEC in Rag1-KO mice and performed i.p. transfer of MDSCs and CD4<sup>+</sup> T cells. Transfer of T cells increased inflammation (Supplementary Fig. 11a) and intestinal permeability (Supplementary Fig. 11b), and decreased survival of mice (Supplementary Fig. 11c). Administration of MDSCs abrogated these effects (Supplementary Fig. 11a–c). Although T cell transfer had a strong effect on mouse survival, it did not affect bacterial load. MDSCs caused a decrease in bacterial load only when mice received T cell transfer (Supplementary Fig. 11d), possibly as a result of decreased NEC severity. Thus, these results indicated that the effect of MDSCs on NEC was mediated via inhibition of T cells.

Induction of NEC was associated with the upregulation of type 17 helper T (T<sub>H</sub>17) cells (IL-17A<sup>+</sup> and Rorγt<sup>+</sup>) in the small intestine. Administration of myeloid cells from AM did not affect that frequency, whereas MDSC from NBM considerably decreased it. MDSCs increased the frequency of Foxp3<sup>+</sup> regulatory T cells (Supplementary Fig. 11e).

LF treatment of WT mice with NEC resulted in the accumulation of MDSCs in the LP (Supplementary Fig. 12a). This effect was associated with decreased intestinal permeability (Supplementary Fig. 12b) and inflammation (Supplementary Fig. 12c), and prolonged survival (Supplementary Fig. 12d). LF decreased the bacterial load in both the intestine and the blood circulation (Supplementary Fig. 12e). In sharp contrast, administration of LF to Rag1-KO mice did not affect the severity of NEC (Supplementary Fig. 12f–h). Administration of T cells enhanced NEC, whereas LF abrogated T cell-induced NEC. Administration of LF had a similar antibacterial effect in mice with or without T cell transfer (Supplementary Fig. 12i). Administration of LF recapitulated the effect of MDSC by downregulating intestinal T<sub>H</sub>17 and upregulating regulatory T cells (Supplementary Fig. 12j).

Thus, in this report, we described the presence of immunosuppressive MDSCs in healthy mice and humans during the first weeks of life. Most of the cells had the phenotype of PMN-MDSCs, a finding consistent with the previously reported elevated numbers of granulocytic MDSCs in infants in the first month of life<sup>20</sup>. However, the presence of MDSCs was not associated with greater myelopoiesis in NBM, because the highest presence of myeloid cells was observed during the first 3 d of life, whereas the immunosuppressive activity of these cells was observed only after day 4. Granulocytes and monocytes from PM lacked suppressive activity. Our data suggested that LF in milk may be responsible for the acquisition of a suppressive phenotype by MDSCs. The suppressive activity of M-MDSCs was mediated by LF-induced NO production, whereas the suppressive activity of PMN-MDSCs involved S100A9-mediated upregulation of PGE2. Our findings were

consistent with a report in humans indicating that LF in the presence of GM-CSF increases S100A9 production<sup>21</sup>. S100A9/A8 proteins have previously been implicated in the regulation of MDSC expansion<sup>22–24</sup>. However, their role in MDSC-mediated suppression was previously unclear. S100A9/A8 in human neutrophils are arachidonic acid (AA)-binding proteins that serve as an intermediate intracellular reservoir for AA and thus modulate the activities of AA-metabolizing enzymes. Higher AA concentrations favor PGE2 production over leukotrienes in neutrophils. This process is mediated by phospholipase A2, which is involved in the Cox-2-mediated generation of PGE2 via microsomal Ptges<sup>25</sup>. Our experiments with S100A9/A8-KO mice demonstrated that *Ptges* expression and PGE2 production are downstream of S100A9/A8. PGE2 directly inhibits the proliferation of T cells via upregulation of cyclic AMP<sup>26</sup>. The effect of LF is cell type dependent, because previous reports have demonstrated that LF negatively regulates PGE2 production in amniotic fluid, enterocytes, and chondrocytes<sup>27–29</sup>. However, these cells lack S100A9/A8 proteins.

We suggest that the presence of MDSCs in newborns may be one mechanism controlling the inflammatory response during the microbial colonization of the gut and lungs. Our data demonstrate the role of MDSCs under steady-state conditions and provide a mechanism for their generation, which appears to be distinct from that involved in cancer. Our results suggest that MDSCs may be used as a potential therapeutic option for treating infants with NEC.

## METHODS

Methods, including statements of data availability and any associated accession codes and references, are available in the [online version of the paper](#).

*Note: Supplementary Information and Source Data files are available in the [online version of the paper](#).*

## ACKNOWLEDGMENTS

This work was supported by the Wistar Institute Animal and Bioinformatics core facilities as well as NIH grant CA165065 to D.I.G. and V.K. The work was also supported by the Recruitment Program for Foreign Experts (Thousand Talents Plan, WQ2014440O204), the Start-up Fund for High-level Talents of Sun Yat-sen University, and the Leading Talents of Guangdong Province Program (D.I.G.). This work was supported by the following grants to J.Z.: the Introduction of Innovative R&D Team Program of Guangdong Province (2009010058), the Guangdong Province Universities and Colleges Pearl River Scholar Funded Scheme (GDUPS, 2014), the National Natural Science Foundation of China (91542112; 81571520, 81771665, and 81742002), and the Provincial Talents Cultivated by the “Thousand-Hundred-Ten” Program of Guangdong Province, 111 Project (B12003). We thank S. Grey-Owen (University of Toronto) and O.M. Conneely (Baylor College of Medicine) for providing LF-KO mice and T. Vogl and J. Roth (Institute of Immunology, Muenster) for providing S100A9-KO mice. We thank Y. Yu (Tianjin Medical University) for providing Cox-2-KO mice and H. Zhang (Sun Yat-sen University) for providing OT-1 transgenic mice.

## AUTHOR CONTRIBUTIONS

Conceptualization, D.I.G. and J.Z.; formal analysis, A.V.K.; investigation, Y.-M.H., X.L., M.P., Y.-E.L., S.-Y.F., Q.-J.Y., Y.-H.Z., and L.W.; resources, Y.N. and E.A.J.; writing original draft, D.I.G. and J.Z.; manuscript review and editing, D.I.G., J.Z., Y.N., and V.K.; supervision, D.I.G. and J.Z.; funding acquisition, D.I.G., J.Z., and V.K.

## COMPETING FINANCIAL INTERESTS

The authors declare no competing financial interests.

Reprints and permissions information is available online at <http://www.nature.com/reprints/index.html>. Publisher's note: Springer Nature remains neutral with regard to jurisdictional claims in published maps and institutional affiliations.

- Marvel, D. & Gabrilovich, D.I. Myeloid-derived suppressor cells in the tumor microenvironment: expect the unexpected. *J. Clin. Invest.* **125**, 3356–3364 (2015).

2. Gabrilovich, D.I. Myeloid-derived suppressor cells. *Cancer Immunol. Res.* **5**, 3–8 (2017).
3. Bronte, V. *et al.* Recommendations for myeloid-derived suppressor cell nomenclature and characterization standards. *Nat. Commun.* **7**, 12150 (2016).
4. Veglia, F., Perego, M. & Gabrilovich, D. Myeloid-derived suppressor cells coming of age. *Nat. Immunol.* <https://doi.org/10.1038/s41590-017-0022-x> (2018).
5. Obermajer, N. *et al.* PGE<sub>2</sub>-driven induction and maintenance of cancer-associated myeloid-derived suppressor cells. *Immunol. Invest.* **41**, 635–657 (2012).
6. Nagaraj, S. *et al.* Antigen-specific CD4<sup>+</sup> T cells regulate function of myeloid-derived suppressor cells in cancer via retrograde MHC class II signaling. *Cancer Res.* **72**, 928–938 (2012).
7. Youn, J.I., Collazo, M., Shalova, I.N., Biswas, S.K. & Gabrilovich, D.I. Characterization of the nature of granulocytic myeloid-derived suppressor cells in tumor-bearing mice. *J. Leukoc. Biol.* **91**, 167–181 (2012).
8. Manitz, M.P. *et al.* Loss of S100A9 (MRP14) results in reduced interleukin-8-induced CD11b surface expression, a polarized microfilament system, and diminished responsiveness to chemoattractants in vitro. *Mol. Cell. Biol.* **23**, 1034–1043 (2003).
9. Park, J.Y., Pillinger, M.H. & Abramson, S.B. Prostaglandin E2 synthesis and secretion: the role of PGE2 synthases. *Clin. Immunol.* **119**, 229–240 (2006).
10. Deshmukh, H.S. *et al.* The microbiota regulates neutrophil homeostasis and host resistance to *Escherichia coli* K1 sepsis in neonatal mice. *Nat. Med.* **20**, 524–530 (2014).
11. Vogel, H.J. Lactoferrin, a bird's eye view. *Biochem. Cell Biol.* **90**, 233–244 (2012).
12. Warner, B.B. & Tarr, P.I. Necrotizing enterocolitis and preterm infant gut bacteria. *Semin. Fetal Neonatal Med.* **21**, 394–399 (2016).
13. Denning, T.L., Bhatia, A.M., Kane, A.F., Patel, R.M. & Denning, P.L. Pathogenesis of NEC: role of the innate and adaptive immune response. *Semin. Perinatol.* **41**, 15–28 (2017).
14. Condamine, T. *et al.* Lectin-type oxidized LDL receptor-1 distinguishes population of human polymorphonuclear myeloid-derived suppressor cells in cancer patients. *Sci. Immunol.* **1**, aaf8943 (2016).
15. Niño, D.F., Sodhi, C.P. & Hackam, D.J. Necrotizing enterocolitis: new insights into pathogenesis and mechanisms. *Nat. Rev. Gastroenterol. Hepatol.* **13**, 590–600 (2016).
16. Condamine, T. *et al.* ER stress regulates myeloid-derived suppressor cell fate through TRAIL-R-mediated apoptosis. *J. Clin. Invest.* **124**, 2626–2639 (2014).
17. James, B.R. *et al.* CpG-mediated modulation of MDSC contributes to the efficacy of Ad5-TRAIL therapy against renal cell carcinoma. *Cancer Immunol. Immunother.* **63**, 1213–1227 (2014).
18. Dominguez, G.A. *et al.* Selective targeting of myeloid-derived suppressor cells in cancer patients using DS-8273a, an agonistic TRAIL-R2 antibody. *Clin. Cancer Res.* **23**, 2942–2950 (2017).
19. Egan, C.E. *et al.* Toll-like receptor 4-mediated lymphocyte influx induces neonatal necrotizing enterocolitis. *J. Clin. Invest.* **126**, 495–508 (2016).
20. Gervasi, A. *et al.* Myeloid derived suppressor cells are present at high frequency in neonates and suppress in vitro T cell responses. *PLoS One* **9**, e107816 (2014).
21. Curran, C.S. & Bertics, P.J. Lactoferrin regulates an axis involving CD11b and CD49d integrins and the chemokines MIP-1α and MCP-1 in GM-CSF-treated human primary eosinophils. *J. Interferon Cytokine Res.* **32**, 450–461 (2012).
22. Cheng, P. *et al.* Inhibition of dendritic cell differentiation and accumulation of myeloid-derived suppressor cells in cancer is regulated by S100A9 protein. *J. Exp. Med.* **205**, 2235–2249 (2008).
23. Heinemann, A.S. *et al.* In neonates S100A8/S100A9 alarmins prevent the expansion of a specific inflammatory monocyte population promoting septic shock. *FASEB J.* **31**, 1153–1164 (2017).
24. Sinha, P. *et al.* Proinflammatory S100 proteins regulate the accumulation of myeloid-derived suppressor cells. *J. Immunol.* **181**, 4666–4675 (2008).
25. St-Onge, M. *et al.* Characterization of prostaglandin E2 generation through the cyclooxygenase (COX)-2 pathway in human neutrophils. *Biochim. Biophys. Acta* **1771**, 1235–1245 (2007).
26. Wehbi, V.L. & Taskén, K. Molecular mechanisms for cAMP-mediated immunoregulation in t cells: role of anchored protein kinase A signaling units. *Front. Immunol.* **7**, 222 (2016).
27. Talukder, J.R., Griffin, A., Jaima, A., Boyd, B. & Wright, J. Lactoferrin ameliorates prostaglandin E2-mediated inhibition of Na<sup>+</sup>-glucose cotransport in enterocytes. *Can. J. Physiol. Pharmacol.* **92**, 9–20 (2014).
28. Trentini, A. *et al.* Vaginal lactoferrin modulates PGE2, MMP-9, MMP-2, and TIMP-1 amniotic fluid concentrations. *Mediators Inflamm.* **2016**, 3648719 (2016).
29. Rasheed, N., Alghasham, A. & Rasheed, Z. Lactoferrin from *Camelus dromedarius* inhibits nuclear transcription factor-κB activation, cyclooxygenase-2 expression and prostaglandin E2 production in stimulated human chondrocytes. *Pharmacognosy Res.* **8**, 135–141 (2016).

## ONLINE METHODS

**Human subjects.** Between September 2016 and October 2017, placental cord blood was collected from women during delivery in the Third Affiliated Hospital of Sun Yat-sen University and the Guangzhou Women and Children's Medical Center, Guangzhou, China. The peripheral blood was collected from infants (0 to 10 d old) delivered in the Third Affiliated Hospital of Sun Yat-sen University (Guangzhou, China) and CHOP in Philadelphia. All subjects were screened for antibodies to serum HIV, hepatitis B surface antigen (HBsAg), antibodies to hepatitis C virus (HCV), hepatitis D virus (HDV) antigen, and antibodies to HDV, and positive individuals were excluded from the study. Women with acute infections (including pneumonia and urinary tract infections) and those with fever were also excluded. Infants presenting with pathologic jaundice, fever, asphyxia neonatorum, and other acute diseases within 7 d after delivery were excluded. Infants with birth weights of 2,500–4,000 g were considered to be of normal weight (NW); those with birth weights <1500 g were considered to be of very low weight (VLW). This study was approved by the Clinical Ethics Review Boards of the Third Affiliated Hospital of Sun Yat-sen University, Guangzhou Women and Children's Medical Center, and CHOP hospital. Written informed consent was obtained from all participants or their legal guardians at the time of admission.

**Flow cytometric analysis of human samples.** PBMCs and cord blood mononuclear cells were isolated from cord blood through Ficoll centrifugation and were analyzed within 6 h after collection. The antibodies used in this study are listed in **Supplementary Table 1**. The cell phenotype was evaluated with an LSRII flow cytometer (BD Bioscience), and data were analyzed in FlowJo V10.0.7 (FlowJo). Data were acquired as the fraction of labeled cells within a live-cell gate set for a minimum of 50,000 events. For the flow cytometric sorting, a BD FACSAria cell sorter (BD Bioscience) was used. The strategy for MDSC sorting was CD14<sup>+</sup>CD11b<sup>+</sup>CD15<sup>+</sup> for PMN-MDSCs and CD11b<sup>+</sup>CD14<sup>+</sup>HLA-DR<sup>low</sup>CD15<sup>+</sup> for M-MDSCs. Examples of gating are provided in **Supplementary Figure 13**.

**Reagents.** Reagents used in the study are listed in **Supplementary Table 2**.

**Mice.** Experiments performed in Sun Yat-sen University (SYSU) were approved by the Institutional Animal Care and Use Committee of Sun Yat-sen University. Experiments performed at the Wistar Institute (WI) were approved by the IACUC of the Wistar Institute. For experiments in SYSU, C57BL/6 and BALB/c mice were purchased from the Laboratory Animal Center of Sun Yat-sen University, and OT-1 transgenic mice were kindly provided by H. Zhang (Sun Yat-sen University). Cox-2-KO mice were kindly provided by Y. Yu (Tianjin Medical University). For experiments at the Wistar Institute, C57BL/6 and BALB/c mice were purchased from Taconic, OT-1 mice were purchased from Jackson Laboratories, S100A9-KO mice were originally provided by J. Roth (University of Munster), Cox-2-KO mice were obtained from Jackson Laboratories, and LF-KO mice were kindly provided by S. Grey-Owen (University of Toronto). All mice were bred in pathogen-free facilities, and age-matched littermates were used as controls.

**Analysis of MDSCs.** Mouse bone marrow cells were harvested through femoral-bone flushing and filtered through a cell strainer (80-µm pore size; Corning). Spleens were mechanically dissociated and filtered. BM cells were cultured in RPMI 1640 medium supplemented with 10% FBS, 20 ng/ml GM-CSF, 20 ng/ml IL-6, and 50 µM 2-ME. The cultures were maintained at 37 °C in a 5% CO<sub>2</sub> humidified atmosphere in 24-well plates. Medium was refreshed on day 3, and cells were analyzed by flow cytometry on day 6. For flow cytometry, red blood cells were lysed in ACK buffer, and cells were stained with the following antibodies: anti-CD11b (BV421, BD), anti-Ly6C (PeCy7, BD), anti-Ly6G (FITC, BD), and Aqua live/dead (Life Technologies) (Catalog and clone numbers are provided in **Supplementary Fig. 1**). Examples of gating are provided in **Supplementary Figure 13**. For PMN-MDSC isolation, cells were labeled with biotinylated anti-Ly6G (Miltenyi), incubated with streptavidin microbeads (Miltenyi), and separated on MACS Columns (Miltenyi). Two passages on columns were done to maximize cell purity. For M-MDSC isolation, CD11b<sup>+</sup>Ly6C<sup>high</sup>Ly6G<sup>+</sup> cells were sorted on a MoFlo AStrios instrument

(Beckman Coulter). All antibodies were obtained from BD Pharmingen. Cell Aqua live/dead (Life Technologies) was used to exclude dead cells. For S100A9 intracellular staining, cells were fixed and permeabilized with CytoFix/CytoPerm solution (BD) according to the manufacturer's instructions, and anti-S100A9 (A647, BD) was used at a 1:200 dilution. ROS were evaluated with DCFDA (Abcam) staining.

**MDSC suppression assay.** PMN-MDSCs were plated in U-bottom 96-well plates (3 replicates) in RPMI with 10% FBS and cocultured at different ratios with splenocytes from Pmel or OT-1 transgenic mice in the presence of cognate peptides: OT-1, SIINFEKL; Pmel, EGSRNQDWL. Cells were incubated for 48 h, and then [<sup>3</sup>H]thymidine (PerkinElmer) was added (1 µl/well) and incubated overnight. Samples were counted with a TopCount NXT instrument (PerkinElmer). To evaluate M-MDSC suppressive activity, sorted CD3<sup>+</sup> T cells from the spleen were labeled with CFSE (2 µM) (Invitrogen), stimulated with anti-CD3 (5 µg/ml)-coated plates and soluble anti-CD28 (1 µg/ml) (eBioscience), and cultured alone or with M-MDSCs at different ratios for 3 d. Cells were then stained with anti-CD4-PE-Cy5 and anti-CD8a-PE, and T-cell proliferation was analyzed by flow cytometry.

**RNA-sequencing data analysis.** PMN-MDSCs and M-MDSCs from spleens of neonatal (7 d old) and adult mice (6 to 8 weeks old) were enriched with CD11b-beads and then sorted on a FACSAria cell sorter (BD Bioscience), on the basis of the CD11b<sup>+</sup>Ly6C<sup>int</sup>Ly6G<sup>+</sup> phenotype for PMN-MDSCs and CD11b<sup>+</sup>Ly6C<sup>high</sup>Ly6G<sup>+</sup> for M-MDSCs. The sorting purity was >95%. RNA sequencing was performed on the Illumina HiSeq 2500 platform. A VAHTS Total RNA-Seq Library Preparation Kit (Vazyme Biotech) was used for library preparation. Single-end-read runs were used with read lengths up to 50 bp in high-output mode and 30 million total read counts. Data were analyzed in RSEM v1.2.12 software<sup>30</sup> against the mm10 genome, and gene-level read counts and RPKM values on the gene level were estimated for the ensemble transcriptome. Samples with at least 80% aligned reads were analyzed. DESeq2 (ref. 31) was used to estimate the significance between any two experimental groups. Overall changes were considered significant at an FDR <5% threshold, and an additional threshold of fold change (>5) was used to generate the final gene set. Gene set enrichment analysis was done with Qiagen's Ingenuity Pathway Analysis software (IPA; <http://www.qiagen.com/ingenuity/>) with the 'functions', 'canonical pathways', 'upstream regulators', and 'networks' options. Gene overlap between microarray and RNA-seq data was assessed on the basis of Entrez IDs and Pearson correlation coefficients calculated between any pair of samples. Each microarray sample correlation value was then normalized to the Pearson correlation versus average RNA-seq profile. RNA-seq data have been deposited in the GEO data repository (accession number GSE97993).

**Quantitative real-time PCR (qRT-PCR).** RNA was extracted with a Total RNA Kit I (Omega) according to the manufacturer's instructions. Primer sequences are listed in **Supplementary Table 3**.

**ELISA.** Cells were cultured 24 h at 2 × 10<sup>6</sup>/ml in RPMI with 10% FBS. PGE<sub>2</sub>, S100A9 or LF ELISA kits (Invitrogen) were used to measure the amounts of corresponding proteins in the cell lysates from 24-h cultures of MDSCs.

**LF treatment.** For *in vivo* experiments, 3-week-old WT and S100A9-KO mice were treated with LF (Sigma Aldrich) (5 mg/mouse i.p. in PBS (vehicle) daily for 8 d), PBS was used as a vehicle control. For *in vitro* treatment, mouse BM cells or cord blood mononuclear cells from VLW babies were cultured in the presence of GM-CSF and IL-6, in the presence or absence of LF protein (700 µg/ml) for 6 d.

**Allergy-induced airway-inflammation mouse model.** BALB/C mice at different ages were intraperitoneally sensitized with 5 µg/g OVA (grade V, Sigma-Aldrich) emulsified in 200 µg/g of aluminum hydroxide (ThermoFisher alum) on days 0 and 7, then intranasally challenged with OVA (5 µg/µl of PBS) once on day 17 to 21. One day after the last challenge, mice were sacrificed, and lung inflammation was examined<sup>32</sup>. For MDSC transfer experiments,

3 million adult spleen neutrophils, neonatal spleen PMN-MDSCs, neonatal spleen M-MDSCs, or vehicle control (PBS) were administered i.v. 1 d before each sensitization.

**Necrotizing enterocolitis (NEC) induction.** NEC induction was performed as previously described<sup>33</sup>. Briefly, neonates were taken from their parents and were fed with formula (Esbilac, PetAg) via oral gavage (100–200  $\mu$ l, three or four times per day) during the observation time. On day 0, mice were gavaged with bacteria obtained from a fecal suspension from adult healthy mouse cecum at  $7 \times 10^7$  CFU/mouse. Starting from day 1, mice were subjected to a hypoxia–cold shock cycle twice per day for 3 d. Mice were placed in a hypoxia chamber at 1% O<sub>2</sub> for 2 min and then immediately transferred to an ice slurry in a precooled bucket for 10 min. After cold shock, mice were returned to their cages and observed for NEC symptoms, including severe abdominal distension, apnea, cyanosis, and lethargy. Small intestines were collected and fixed in 10% buffered formalin for histological examination. Fluorescein isothiocyanate (FITC)-labeled dextran (FD7000; molecular weight 73,000) (Sigma-Aldrich) was used to assess mucosal permeability, as described previously<sup>34</sup>.

In MDSC depletion experiments, 40  $\mu$ g/g of anti-DR5 (BioXcell) was administered to 6-d-old neonates i.p. 1 h before and 36 h after initiation of the NEC procedure. Rat IgG isotype was used as a control. To induce NEC in KO mice, 6-d-old mice (WT, S100a9 KO, or Rag1 KO) were used. In MDSC transfer experiments, 1 million neonatal spleen Gr-1<sup>+</sup> cells per mouse were administered i.p. 1 h before initiation of the NEC procedure, and adult mouse spleen Gr-1<sup>+</sup> cells and vehicle (PBS) were used as controls. For T cell transfer in Rag1-KO mice,  $4 \times 10^6$  spleen CD4<sup>+</sup> T cells from NEC mice were used. In the LF treatment group, LF (0.25g/kg in PBS) was administered to 1-d-old neonates by i.p. injection daily 1 h before the NEC procedure until the end of the experiment.

**qPCR measurement of bacterial loading.** DNA was extracted from the serum and intestine, and the total amount of bacterial sRNA was then quantified with bacteria-specific 16S primers, as described previously<sup>35</sup>.

**Cross-fostering.** Breeding pairs of WT and LF-KO mice were concurrently set up when adults were 5 to 6 weeks old. Only litters born on the same day were included in the cross-fostering experiments. After delivery, a WT adult female was removed from her cage and placed with an LF-KO litter, and vice versa. Fostered pups were maintained until day 7 after birth, then sacrificed for functional tests.

**Statistics.** In most experiments, statistical analyses were done with two-tailed unpaired Student's *t* tests. Where indicated, nonparametric Mann–Whitney tests were used. Survival curves were compared with the log-rank (Mantel–Cox) test and Gehan–Breslow–Wilcoxon tests. Statistical tests were performed in GraphPad Prism version 7.0 and SPSS Statistics 20.0. *P* values <0.05 were considered significant. RNA-seq data were analyzed in RSEM v1.2.12 software, DESeq2, and Ingenuity Pathway Analysis software.

**Life Sciences Reporting Summary.** Further information on experimental design is available in the **Life Sciences Reporting Summary**.

**Data availability.** The RNA-seq data set has been deposited in the GEO data repository (accession number [GSE97993](https://www.ncbi.nlm.nih.gov/geo/query/acc.cgi?acc=GSE97993)).

30. Li, B. & Dewey, C.N. RSEM: accurate transcript quantification from RNA-Seq data with or without a reference genome. *BMC Bioinformatics* **12**, 323 (2011).
31. Love, M.I., Huber, W. & Anders, S. Moderated estimation of fold change and dispersion for RNA-seq data with DESeq2. *Genome Biol.* **15**, 550 (2014).
32. Mosconi, E. *et al.* Breast milk immune complexes are potent inducers of oral tolerance in neonates and prevent asthma development. *Mucosal Immunol.* **3**, 461–474 (2010).
33. Tian, R. *et al.* Characterization of a necrotizing enterocolitis model in newborn mice. *Int. J. Clin. Exp. Med.* **3**, 293–302 (2010).
34. Rager, T.M., Olson, J.K., Zhou, Y., Wang, Y. & Besner, G.E. Exosomes secreted from bone marrow-derived mesenchymal stem cells protect the intestines from experimental necrotizing enterocolitis. *J. Pediatr. Surg.* **51**, 942–947 (2016).
35. Kubinak J.L. *et al.* MyD88 signaling in T cells directs IgA-mediated control of the microbiota to promote health. *Cell Host Microbe* **17**, 153–163 (2015).

## Life Sciences Reporting Summary

Nature Research wishes to improve the reproducibility of the work we publish. This form is published with all life science papers and is intended to promote consistency and transparency in reporting. All life sciences submissions use this form; while some list items might not apply to an individual manuscript, all fields must be completed for clarity.

For further information on the points included in this form, see [Reporting Life Sciences Research](#). For further information on Nature Research policies, including our [data availability policy](#), see [Authors & Referees](#) and the [Editorial Policy Checklist](#).

### ► Experimental design

#### 1. Sample size

Describe how sample size was determined.

For in vitro exploratory experiments 3-5 independent biological replicates was used. No calculation of sample size estimation was performed. For in vivo experiment calculation of sample size was made based on expected survival of mice with NEC during first week of life. We used confidence level of 95%.

#### 2. Data exclusions

Describe any data exclusions.

No animals or samples were excluded from the analysis.

#### 3. Replication

Describe whether the experimental findings were reliably reproduced.

All experiments were reproduced. In each figure the number of replicates were stated and sample size was provided. Many experiments in two laboratories (one in China and one in the US) were performed in parallel by independent investigators who obtained similar results.

#### 4. Randomization

Describe how samples/organisms/participants were allocated into experimental groups.

For all in vivo experiments, mice were randomized for sex and weight to have even groups between treated and control.

#### 5. Blinding

Describe whether the investigators were blinded to group allocation during data collection and/or analysis.

Investigators were no blinded, since it was not feasible due to the nature of experiments.

Note: all studies involving animals and/or human research participants must disclose whether blinding and randomization were used.

#### 6. Statistical parameters

For all figures and tables that use statistical methods, confirm that the following items are present in relevant figure legends (or the Methods section if additional space is needed).

n/a Confirmed

- |                          |                                     |  |
|--------------------------|-------------------------------------|--|
| <input type="checkbox"/> | <input checked="" type="checkbox"/> | The <u>exact</u> sample size ( $n$ ) for each experimental group/condition, given as a discrete number and unit of measurement (animals, litters, cultures, etc.)                                    |
| <input type="checkbox"/> | <input checked="" type="checkbox"/> | A description of how samples were collected, noting whether measurements were taken from distinct samples or whether the same sample was measured repeatedly.  |
| <input type="checkbox"/> | <input checked="" type="checkbox"/> | A statement indicating how many times each experiment was replicated   |
| <input type="checkbox"/> | <input checked="" type="checkbox"/> | The statistical test(s) used and whether they are one- or two-sided (note: only common tests should be described solely by name; more complex techniques should be described in the Methods section) |
| <input type="checkbox"/> | <input checked="" type="checkbox"/> | A description of any assumptions or corrections, such as an adjustment for multiple comparisons  |
| <input type="checkbox"/> | <input checked="" type="checkbox"/> | The test results (e.g. $p$ values) given as exact values whenever possible and with confidence intervals noted   |
| <input type="checkbox"/> | <input checked="" type="checkbox"/> | A summary of the descriptive statistics, including central tendency (e.g. median, mean) and variation (e.g. standard deviation, interquartile range)   |
| <input type="checkbox"/> | <input checked="" type="checkbox"/> | Clearly defined error bars   |

See the web collection on [statistics for biologists](#) for further resources and guidance.

## ► Software

Policy information about [availability of computer code](#)

### 7. Software

. RNAseq data were analyzed by RSEM v1.2.12 software, DESeq2, Ingenuity® Pathway Analysis software.

Describe the software used to analyze the data in this study.

Statistical tests were performed using GraphPad Prism version 7.0 and SPSS Statistics 20.0.

For all studies, we encourage code deposition in a community repository (e.g. GitHub). Authors must make computer code available to editors and reviewers upon request. The *Nature Methods* [guidance for providing algorithms and software for publication](#) may be useful for any submission.

## ► Materials and reagents

Policy information about [availability of materials](#)

### 8. Materials availability

Indicate whether there are restrictions on availability of unique materials or if these materials are only available for distribution by a for-profit company.

No unique material was used

### 9. Antibodies

Describe the antibodies used and how they were validated for use in the system under study (i.e. assay and species).

More than 20 different antibodies were used in the study. They are all listed in Supplemental Table 2. They were all commercial antibodies with validation procedures described on the sites of the companies.

### 10. Eukaryotic cell lines

a. State the source of each eukaryotic cell line used.

No cell lines were used. Experiments were performed with primary cells.

b. Describe the method of cell line authentication used.

No cell lines were used.

c. Report whether the cell lines were tested for mycoplasma contamination.

No cell lines were used.

d. If any of the cell lines used in the paper are listed in the database of commonly misidentified cell lines maintained by [ICLAC](#), provide a scientific rationale for their use.

No cell lines were used.

## ► Animals and human research participants

Policy information about [studies involving animals](#); when reporting animal research, follow the [ARRIVE guidelines](#)

### 11. Description of research animals

Provide details on animals and/or animal-derived materials used in the study.

Experiments performed in Sun Yat-sen University (SYSU) were approved by the Institutional Animal Care and Use Committee of Sun Yat-sen University. Experiments performed at Wistar Institute (WI) were approved by IACUC of the Wistar Institute. For experiments in SYSU, C57BL/6 and BALB/c mice were purchased from the Laboratory Animal Center of Sun Yat-sen University and OT-1 transgenic mice were kindly provided by Dr. Hui Zhang (Sun Yat-sen University). Cox-2 KO mice were kindly provide by Dr. Ying Yu (Tianjin Medical University). For experiments at WI, C57BL/6 and BALB/c mice were purchased from Taconic, OT-1 mice from Jackson Lab, S100A9 KO mice were originally provided by Dr. J. Roth (University of Munster), Cox-2 KO mice were obtained from Jackson Lab, LF KO mice were kindly provided by Dr. Grey-Owen (University of Toronto). All mice were bred in pathogen-free facilities, and age-matched littermates were used as controls.

Females mice were used in most experiments. For adult mice (AM), 6-8 weeks mice were used, for newborn mice (NBM), 1-2 weeks mice were used. detailed ages were indicated in each experiment.

## 12. Description of human research participants

Describe the covariate-relevant population characteristics of the human research participants.

Between September 2016 and October 2017, placental cord blood was collected from women during delivery in the Third Affiliated Hospital of Sun Yat-sen University, and Guangzhou Women and Children's Medical Center, Guangzhou, China. The peripheral blood was collected from infants (aged day 0 to 10) delivered in the Third Affiliated Hospital of Sun Yat-sen University (Guangzhou, China) and CHOP in Philadelphia. All subjects were screened for serum HIV antibody, hepatitis B surface antigen (HBsAg), hepatitis C virus (HCV) antibody, hepatitis D virus (HDV) antigen, and HDV antibody and positive individuals were excluded from the study. Women with acute infections (including pneumonia, urinary tract infection) and those with fever were also excluded. Infants presented pathologic jaundice, fever, asphyxia neonatorum and other acute diseases within 7 days after delivery were excluded. Infants born with 2500g-4000g were defined as normal weight (NW), lower than 1500g was considered to be very low weight (VLW). This study was approved by the Clinical Ethics Review Board of the Third Affiliated Hospital of Sun Yat-sen University, Guangzhou Women and Children's Medical Center, and CHOP hospital. Written informed consent was obtained from all the participants or their legal guardians at the time of admission.

## Flow Cytometry Reporting Summary

Form fields will expand as needed. Please do not leave fields blank.

### ► Data presentation

For all flow cytometry data, confirm that:

- ☒ 1. The axis labels state the marker and fluorochrome used (e.g. CD4-FITC).
- ☐ 2. The axis scales are clearly visible. Include numbers along axes only for bottom left plot of group (a 'group' is an analysis of identical markers).
- ☒ 3. All plots are contour plots with outliers or pseudocolor plots.
- ☒ 4. A numerical value for number of cells or percentage (with statistics) is provided.

### ► Methodological details

5. Describe the sample preparation.

Peripheral blood mononuclear cells (PBMC) were isolated by Ficoll centrifugation. Prior to staining with fluorochrome-conjugated antibodies, red blood cells were lysed by adding 1 ml ACK buffer.

6. Identify the instrument used for data collection.

7. Describe the software used to collect and analyze the flow cytometry data.

8. Describe the abundance of the relevant cell populations within post-sort fractions.

9. Describe the gating strategy used.

Cells were obtained from spleens or lamina propria as indicated in the figures and text. Spleen cells were evaluated after lysis of red cells, lamina propria tissues were first enzymatically digested as indicated in methods. In humans periphery blood and cord blood cells were used directly.

LSRII flow cytometer (BD Bioscience). For the flow cytometric sorting, a BD FACSAria cell sorter (BD Bioscience) was used.

FlowJo V10.0.7 (FlowJo, OR, USA)

Data were acquired as the fraction of labeled cells within a live-cell gate set for minimum 50,000 events.

All relevant information was provided in manuscript. Gating strategy was shown in separate supplementary figures. **Supplementary Fig.13**

Tick this box to confirm that a figure exemplifying the gating strategy is provided in the Supplementary Information. ☒

Gating based on FSC area vs width and SSC area vs height and live/dead staining were used to gate live, single cells. Gates were drawn as shown in the relevant panels. Positive and negative population were defined by using fluorescence minus one controls, or appropriate positive and negative controls. For MDSC gating strategy, we followed Nat Commun. 2016 Jul 6;7:12150.

## Editorial Policy Checklist

This form is used to ensure compliance with Nature Research editorial policies related to research ethics and reproducibility in the life sciences. For further information, please see our [Authors & Referees](#) site. All questions on the form must be answered.

### ► Data availability

Policy information about [availability of data](#)

#### Data availability statement

All manuscripts must include a [data availability statement](#). This statement should provide the following information, where applicable:

- Accession codes, unique identifiers, or web links for publicly available datasets
- A list of figures that have associated source data
- A description of any restrictions on data availability

☒ A full data availability statement is included in the manuscript.

#### Required accession codes

Data deposition is mandated for [certain types of data](#).

Confirm that all relevant data have been deposited into a public repository and that all accession codes are provided.

☒ Accession codes will be available prior to publication ☐ No data with mandated deposition ☐ All relevant accession codes are provided

### ► Data presentation

#### Image integrity

☒ Confirm that all images comply with our [image integrity policy](#).

Unprocessed data must be provided upon request. Please double-check figure assembly to ensure that all panels are accurate (e.g. all labels are correct, no inadvertent duplications have occurred during preparation, etc.).

#### Data distribution

Data should be presented in a format that shows data distribution (dot-plots or box-and-whisker plots), with all box-plot elements (e.g. center line, median; box limits, upper and lower quartiles; whiskers, 1.5x interquartile range; points, outliers) defined. Bar graphs should be used only when there is no other viable option for data presentation.

☒ Confirm that all data presentation meets these requirements.

☒ Confirm that in all cases where the number of data points is <10, individual data points are shown.

### ► Structural data

Policy information about [special considerations](#) for specific types of data

☒ If this study did not involve data of these types, check here and skip the rest of this section.

#### Crystallographic data

☐ For all reports of new three-dimensional structures of small molecules, confirm that you have provided a .cif file and a structural figure with probability ellipsoids for publication as Supplementary Information.

#### Macromolecular structures

☐ For all macromolecular structures studied, confirm that you have provided an official validation report from [wwPDB](#).

#### Electron microscopy

☐ For all electron microscopy work, confirm that you have deposited any density maps and coordinate data in [EMDB](#).

### ► Code availability

Policy information about [availability of computer code](#)

#### Code availability statement

For all studies using custom code, the Methods section must include a statement under the heading "Code availability" describing how readers can access the code, including any restrictions to access.

☐ A full code availability statement is included in the manuscript ☒ No custom code used

## ► Research animals

Policy information about [studies involving animals](#); follow the [ARRIVE guidelines](#) for reporting animal research

☐ If this study did not use animals and/or animal-derived materials for which ethical approval is required, check here and skip the rest of this section.

### Ethical compliance

☒ Confirm that you have complied with all relevant ethical regulations and that a statement affirming this is included in the manuscript.

### Ethics committee

☒ Confirm that you have stated the name(s) of the board and institution that approved the study protocol in the manuscript.

## ► Human research participants

Policy information about [studies involving human research participants](#)

☐ If this study did not involve any human research participants, check here and skip the rest of this section.

### Ethical compliance

☒ Confirm that you have complied with all relevant ethical regulations and that a statement affirming this is included in the manuscript.

### Ethics committee

☒ Confirm that you have stated the name(s) of the board and institution that approved the study protocol in the manuscript.

### Informed consent

☒ Confirm that informed consent was obtained from all participants.

### Identifiable images

For publication of identifiable images of research participants, confirm that consent to publish was obtained and is noted in the Methods.

Authors must ensure that consent meets the conditions set out in the [Nature Research participant release form](#).

☐ Yes ☒ No identifiable images of human research participants

## ► Clinical studies

Policy information about [clinical studies](#)

☒ If this study was not a clinical trial, check here and skip the rest of this section.

### Clinical trial registration

☐ Confirm that you have provided the trial registration number from [ClinicalTrials.gov](#) or an equivalent agency in the manuscript.

### Phase 2 and 3 randomized controlled trials

Confirm that you have provided the [CONSORT checklist](#) with your submission.

☐ Yes ☐ No ☐ Not a phase 2/3 randomized controlled trial

### Tumor marker prognostic studies

Did you follow the [REMARK reporting guidelines](#)?

☐ Yes ☐ No ☐ Not a tumor marker prognostic study

## ► Methods reporting

Nature Research wishes to improve the reproducibility of the work we publish. As part of this effort, all life science manuscripts require a [reporting summary](#); certain types of research require specialized modules in addition to this form.

☒ Confirm that you have provided a complete and accurate [reporting summary](#).

n/a | Confirmed

☒ ☐ For MRI studies, confirm that you have completed the additional [MRI module](#).

☐ ☒ For flow cytometry studies, confirm that you have completed the additional [flow cytometry module](#).

☒ ☐ For ChIP-seq studies, confirm that you have completed the additional [ChIP-seq module](#).

I certify that all the above information is complete and correct.

Typed signature Dmitry Gabrilovich

Date Nov 15, 2017

